ORIGINAL ARTICLE

Design of a structurally welded/adhesively bonded joint between a fiber metal laminate and a steel plate for marine applications

Mario de Vicente[1] · Arturo Silva-Campillo[1] · Miguel Ángel Herreros[1,2] · Juan Carlos Suárez-Bermejo[2]

Abstract

Shipbuilding with steel elements has changed little over the past 100 years. The introduction of hybrid materials has led to certain changes in construction methodology and in the calculation of structure and fabrication in shipyards. This study assesses a welded/adhesively joint used as a primary element union. It is made of steel and is used with a hybrid panel that is easy to manufacture and install at a low cost. To define the geometry of the joint, topological optimization of a symmetrical clamp-shaped steel part is carried out, attaching the hybrid panel with a structural adhesive. The geometric shape resulting from this optimization is analysed with a finite element model by means of a non-linear *cohesive zone model* simulation, minimizing the Von Mises stresses. The numerical result is compared to a destructive laboratory test. The result is analysed using the digital image correlation technique, making the following validations: in the adhesive-bonded area, no damage was found; the structural failure begins in the area near the embedded end; and there is an absence of cracks since no debonding of the structural adhesive takes place, confirming the obtained design by numerical simulation.

Keywords Unsymmetrical bonded joint · Hybrid joints · Composite-to-steel joints · Debonding · Cohesive Zone Model

1 Introduction

At the onset of the twentieth century, structural elements were attached by welding, instead of the "clinker and carvel" construction of the late nineteenth century [1]. This change was brought about by the onset of steel construction, with the change in materials leading to a change in how they are attached, from wood (clinker and carvel) to iron (riveted) and iron to steel (welded).

Nowadays the method used for shipbuilding is to manufacture the block upside-down, the welded assemblies were used, and have to be erected [2]. The use of hybrid materials as construction materials helps for the building of the block in position, without the need for erection, using hybrid

panels that are joined together with the primary members of the structure, these panels will replace the actual stiffened steel plates used [3]. The conventional structural construction system should be replaced by a different one, defined here as a "panelized" system, Fig. 1. The innovative combination of both materials and joints has led to a new method of shipbuilding, it is the next step in the evolution, and it will affect the construction method.

Due to the subdivision of works by departments, hull, outfitting, or piping, the construction strategy used in shipyards should clearly be modified. The benefits produced in the hull department by a panelized structure are more than evident, avoiding ordinary stiffeners, profile steps and ties, while simultaneously saving time and welding costs. In the outfitting discipline, pipes and ducts can be routed without bends and elbows, avoiding ordinary stiffeners. HVAC (Heating-Ventilation and Air Conditioning) ducts can be installed near the deck. The free height for passengers and crew can be increased [4], and, alternatively, when insulation is in place, the number of square meters and folds can be minimized in a panel system, thanks to the lack of stiffeners.

Currently, the use of hybrid metallic and composite materials is limited to a small area of the vessel, such as

✉ Mario de Vicente
mario.devicente@upm.es

1   Department of Naval Architecture, Shipbuilding and Ocean Engineering, Universidad Politécnica de Madrid (UPM), Madrid, Spain

2   Department of Material Science, Structural Materials Research Centre (CIME), Universidad Politécnica de Madrid (UPM), Madrid, Spain
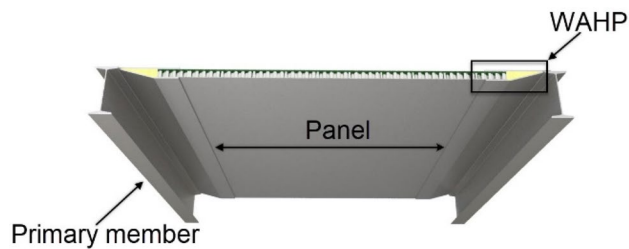
Fig. 1 Panelized system. Primary members with the panel joint by means of the WAHP

helicopter decks [5] or small car decks, since the problem of joints between the hybrid materials and the structure remains to be solved or solutions (laser joints) are too costly and the quality checking procedure of laser welds during manufacturing [6]. Furthermore, the Classification Societies attempted to develop rules for the calculation of hybrid panels [7], but the joints between primary elements and panels are considered in a very limited manner, by means of rivets or bolts. Therefore, the development of a mixed joint between the hybrid material and the steel structure is clearly needed, specifically one that is simple, low-priced, and easy to assemble. This joint is the most delicate point in the use of these materials in shipbuilding.

The need for new materials in shipbuilding has risen from the increasing weight of these structures. Reducing this weight without compromising structural integrity is essential, and currently, the use of aluminium alloys or high strength steels is the best method for reducing weight. These materials can be found in hybrid combinations, such as aluminium honeycomb sandwich or fiber-reinforced panels. When using a hybrid panel, weight is reduced, and the potential benefits of these lighter materials are evident in terms of the following aspects:

First, when the weight of a superstructure is reduced [8], its stability improves, due to the reduced height of the center of gravity above the keel [9]. The risk of capsizing is reduced as well, and the vessel can increase its payload, resulting in higher revenues. Second, shipyard fabrication costs are reduced for the erected construction site, with a reduction in meters of welding, piping, and stiffeners, and, therefore, initial costs. These decreased initial costs and increased operating revenue lead to better investment returns in a shorter amount of time.

In the light of new technological developments, and in the context of panelization, it is possible to answer the question of whether or not conventional ships can be built using hybrid structures. The use of composite materials in shipbuilding tends to take place only in small pleasure yachts, 30–50 feet in length, or in military ships. For example, the world's largest minesweeper, measuring 62 m in length, is made of composite materials [10, 11]. The use

of hybrid materials in shipbuilding has been studied by some authors and class societies have attempted to update their rules based on the new technology [12, 13]. One of the main challenges in these studies concerns the panel-to-panel, primary elements-to-panel, and ordinary stiffeners-to-panel joints. Some of these studies include the use of laser welding [6, 14], but this technology is difficult to use in all shipyards due to certain disadvantages, including equipment, environmental control of the process, and the need for certified welders. The welding of hybrid panels introduces an additional problem: temperature, since the heat transmitted through the sheets can render the hybrid material unusable.

This study focuses on the design of the joint positioned between the panel and primary elements. To date, studies have considered the overall replacement of the ship without modifying the constructive system, and the joining methods used are solved by laser welding or even, by riveting [5], but not with adhesive. The use of structural adhesive on panels is common in the aerospace and industrial sector, but not in marine engineering. In these fields, studies of steel-composite adhesive joints subjected to uni/bi-axial loading are carried out using different definitions of the adhesive layer constitutive ratio Cohesive Zone Model or the Embedded Process Zone (the CZM or EPZ [15]).

On the other hand, fatigue analysis performed in other disciplines [16, 17] can guide a further study within the WAHP, considering its geometry, and its behaviour.

The complete replacement of the structural system through a panelization system involves an easy methodology of making the joints between panels and the primary structural elements, which are made of steel. Therefore, the work is performed in two distinct steps: first, the numerical approach to the structural joint, and second, the verification of the simulation through laboratory tests. At the end of the work, both results must be verified to validate the numerical calculation and the solution developed.

The numerical study and defining of the *Welded-Adhesively Hybrid Panel joint* (hereinafter WAHP) is carried out with two different models: a 2D/3D linear-solid model, and a 2D non-linear model. The first model considers topological optimization to minimize weight, while the second relies on parameter modification by minimizing the Von Mises stress using a 2D CZM model for the joint-panel interface. Nine-node 2D plane strain elements are used, and the adhesive material is modelled using zero-thickness interface elements. In this case, the bond between the WAHP and the panel was first simulated using a structural adhesive. Then, numerical simulations were performed using a soft one. The result of the topological optimization is the input for the non-linear CZM simulation, and its result leads to the geometry used in the laboratory test to verify the study's validity.

2 Methodology

The basic joint design (see Fig. 2) consists of a metal tongue, two adhesive layers and a composite panel, *Mateglass,* consisting of layers of mat, woven and Procore (further details are shown in *Testing Method*). The joint was clamped at the top (red bar in Fig. 2), since ship decks and bulkheads are required to have a smooth face. The far end was subject to a fixed forced displacement to simulate the loading in which the panel will be working. Furthermore, to avoid construction handicaps, the joint geometry must be defined according to the following assumption: easy to produce, easy to install, widely available to all shipyards, and low cost. These assumptions influence the decisions and results of each phase. The materials used for the simulations are the same as those used in the laboratory test.

ANSYS Workbench was used for the numerical simulation and the NCorr code [18] was used for data processing and image correlation. The algorithm identifies the location of each control point on the specimen and tracks them. Post-processing of the results was carried out in Matlab and Excel.

2.1 Topological optimization

The WAHP was designed, optimized, and tested with an assumed displacement at the far edge of the clamped area. Initially, a steel block with the dimensions shown in Fig. 2 and Table 1 was adopted as the initial geometry for the WAHP. The objective was to reduce the mass of this component, eliminating all non-working materials.
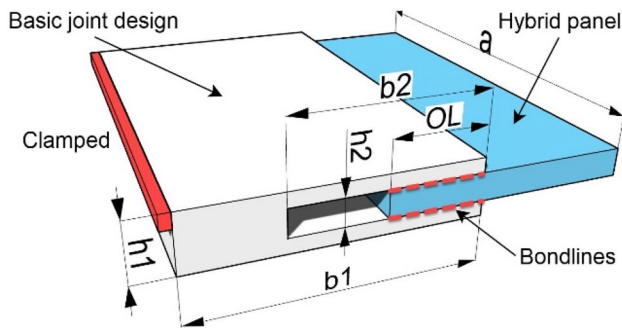

Fig. 2 Geometry sketch—Initial block of two tongues
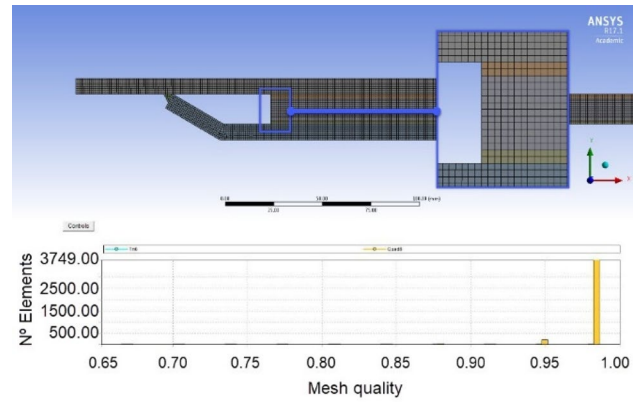

Fig. 3 Mesh quality for numerical simulation

To solve the problem at this stage of the study, it was assumed that the left edge of the WAHP was perfectly clamped at the top, and the joint between the top and bottom faces of the panel with the steel sheets were perfectly bonded. The objective function of the optimization problem to be solved is defined as the total mass of the steel part (*W*), which should be as light as possible (Eq.1):

$$W = a\rho\left(b_1 h_1 - b_2 h_2\right) \tag{1}$$

2D and 3D topological optimization model: Initially, the optimization was performed on a 2D plane stress model. The objective function is the same as shown in Eq. 1. The values set in the analysis properties for the part depth (*a*) ranged from 2100 to 5 mm, and the contact definition between the part and the panel was bonded. Subsequently, the same topological optimization was carried out through 3D linear static analysis. For this, the conditions adopted in the previous 2D study were maintained. The main objective of this analysis was to determine the main differences, if any, from the 2D analysis.

The finite element mesh was generated considering a maximum element size of 5 mm, with a face meshing control, for the steel area, and a maximum element size of 15 mm for the rest of the bodies. To evaluate element quality, the shape of each element of the model was computed to compare the area/volume of the element with a regular one, where a value of 1 indicates a perfect cube or square [19], the minimum element quality of the whole model is 0.651, located near the weld, and the average of the whole model is 0.992, according to the yellow bar shown in Fig. 3. The mesh quality for the whole WAHP block is approximately equal to one.

Table 1 Data seed for topological optimization

	a (mm)	b_1 (mm)	h_1 (mm)	b_2 (mm)	h_2 (mm)	*t* (mm)	OL (mm)
2D Model	2100–50	200	31	100	15	8	50
3D Model	250	200	31	70	15	8	50

2D and 3D linear-solid elements were used. The objective range was a weight reduction of a minimum of 30% and a maximum of 70%. The main geometrical parameters of the WAHP should not be defined a priori. The working panel selected was Mateglass and was used for the topological optimization procedure, to define the geometry. This optimization should not depend on the hybrid material, as long as it individually supports the load, so different material models can be also used during the design phase, with similar results [20].

The result of this analysis is used as input for the following simulation, and according to the design assumptions, the connection is made with steel plates, since they are easily supplied by the shipyards, and avoid the use of more expensive castings. The geometry resulting from this analysis can be seen in Fig. 4.

2.2 Non-linear simulation and parameter definition

Once the geometry of the joint part was defined with two steel plates welded together and the adhesive with the hybrid panel, we proceeded to study the joint's structural behaviour. This refers to all of the stresses being transferred to the WAHP through the adhesive interface. The objectives of this approach were to minimize the local and global Von Mises stress (it had not yet been an objective of the simulation). Simultaneously, the control points of the upper and lower lip were arranged in the areas where the debonding began. For this minimization, we proceeded to vary the joint dimensions according to the parameters defined in Fig. 4. Table 2 shows the initial seed and the variation ranges of the parameters. The hybrid panel width was 3 layers for a total of 9 mm, and the plate thickness was 4 mm.

The study of the adhesive zone between the WAHP and the hybrid panel was the main challenge, so the mathematical model had to be consistent with the physical phenomenon. Of the available fracture mechanics calculation theories, linear elastic fracture mechanics (LEFM) was used based on its ability to model the physical process of the joint, based on the analysis of cracks and combines the numerical and experimental analysis of fracture.

Of all of the approaches to adhesive bond models [21, 22], one, the so-called Cohesive Zone Model, is based on the application of finite elements to the bonded joints. It is
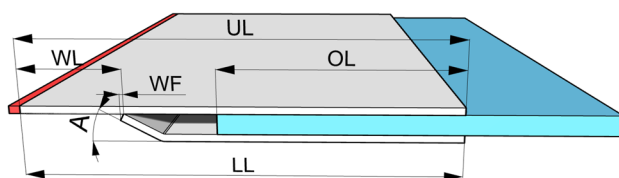
Table 2 Initial seed and range of parameters

Name	Code	Seed	Type	Lower limit	Upper limit
Angle	A	30º	Angle	15	45º
Upper length	UL	200 mm	Length	180	250
Overlap	OL	100 mm	Length	90	175
Weld location	WL	50 mm	Length	10	55
Lower length	LL	200 mm	Length	200	225
Weld foot	WF	4.9 mm	Length	4.24	7.8

frequently used in debonding analysis. This analysis has no geometric limitations (only a calculation time limitation) and is based on Linear Elastic Fracture Mechanics (LEFM). This method does not model the adhesive based on elements and it transmits the stresses via fracture mechanics and crack propagation.

The study of the two parts (materials bonded together) and the cohesive material is treated as a crack expanding between them. The crack propagates and the materials begin to separate as a fracture occurs. The constitutive relationship between the traction T and the corresponding interlayer separation δ that guides this approach is shown in Fig. 5 (blue line).

Damage begins when the stress reaches a limiting value σ_{max}. The damage process progresses, and the stress decreases to zero before the actual fracture occurs at the critical displacement U_n^c. The adhesive's behaviour is simplified, according to Fig. 5, bilinear cohesion law [23] (red line on the graph), whose main characteristics are: the load follows a linear function until reaching the maximum in stress (OA) and then descends following another linear function (AC), the area under the OAC curve represents the critical fracture energy, including the damage, so when unloading occurs, it follows the OB trajectory.
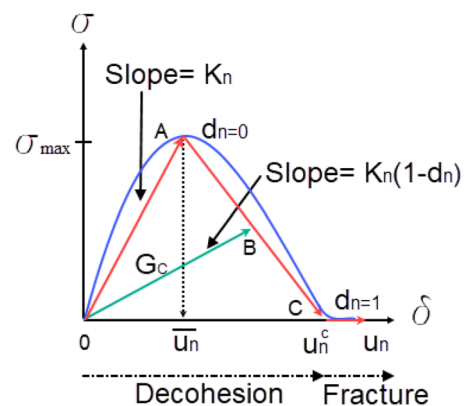

Fig. 4 Definition of the WAHP parameters

Fig. 5 Bilinear CZM law representing adhesive stress vs. relative displacement

Of the three different failure modes of calculation, Mode I is dominated by the normal displacement to the interface. Mode II is governed by a tangential slip. And in the Mixed Mode, the interface depends on both normal and tangential components. The last one, Eq. 2 has been chosen. Here, G_{cn} (Eq. 3) and G_{ct} (Eq. 4) are the critical fracture energies for Mode I and Mode II, respectively. In the Mixed Mode, both the normal and tangential components are involved in interface debonding, and hence the debonding parameter is defined in Eq. 5. The rest of the parameters are shown in Fig. 5.

$$\left[\frac{G_n}{G_{cn}}\right]^2 + \left[\frac{G_t}{G_{ct}}\right]^2 = 1 \tag{2}$$

$$G_{cn} = \int_0^{u_n^c} P\,du = \frac{1}{2}\sigma_{\max}u_n^c \tag{3}$$

$$G_{ct} = \int_0^{u_t^c} T\,du = \frac{1}{2}\tau_{\max}u_t^c \tag{4}$$

$$d_m = \left(\frac{\sqrt{\left(\frac{u_n}{\vec{u}_n}\right)^2 + \left(\frac{u_t}{\vec{u}_t}\right)^2} - 1}{\sqrt{\left(\frac{u_n}{\vec{u}_n}\right)^2 + \left(\frac{u_t}{\vec{u}_t}\right)^2}}\right)\left(\frac{u_n^c}{u_n^c - \vec{u}_n}\right) \tag{5}$$

Numerical analysis of the debonding may face convergence difficulties. Therefore, an extra parameter (η) is included in the t-step, as follows:

$$\sigma = \sigma^{\text{final}} + \left(\sigma^{\text{initial}} - \sigma^{\text{final}}\right)e^{\frac{-t}{\eta}} \tag{6}$$

After separating the two bonded materials, the defined contact behaviour between the two surfaces begins.

2.3 Non-linear model

All of the described geometrical parameters were included in the parametric study. This study was non-linear and the CZM bilinear constitutive law was used. Contact nonlinearity and fracture mechanics approaches were used to simulate the cohesion zone using the mixed separation mode. In this mode, interface separation depends on the normal and tangential components. The sample consisted of 50 numerical experiments, and to achieve a satisfactory design, the Von Mises stress must be minimized, and adhesive delamination effects must be assessed.

To perform Goal Driven Optimization (GDO) in a finite element analysis framework, it is useful to perform a Design of Experiments (DOE) study beforehand. From the DOE study, a response surface is constructed, and then the GDO can be executed and evaluated. In a DOE study, when the input parameters increase, the sampling points required for the analysis increase dramatically. Initially, an analysis is performed with all parameters, making it possible to identify which parameters are the most sensitive, and to reduce any unnecessary sampling points.

Correlation of parameters: The cost of solving an operational optimization problem using finite elements can be very high when the model is large and, therefore, it is important to determine the model's sensitivity to the different parameters. To calculate the correlation matrix, a previous DOE study was carried out. This analysis allows the exclusion of unimportant parameters.

The generation of value samples is usually based on the Latin Hypercube Sampling (LHS) method, which generates samples having a correlation tolerance of 5%. An advanced variant of this method, the Optimal Space Filling (OSF), was used for sampling to maximize the distance between samples.

The parametric correlation theory used was Spearman's rank correlation, defined in Eq. 7, in which the numerator is the covariance of the rank variables, and the denominator is the multiplication of the standard deviations. It is distributed by the Student's t with $n = n - 2$ degrees of freedom and with t being the correlation coefficient and B, the beta function, Eq. 8.

$$r_s = \frac{\sum_i^n \left(R_i - \vec{R}\right)\left(S_i - \vec{S}\right)}{\sqrt{\sum_i^n \left(R_i - \vec{R}\right)^2}\sqrt{\sum_i^n \left(S_i - \vec{S}\right)^2}} \tag{7}$$

$$A(t|v) = \frac{1}{\sqrt{v}B\left(\frac{1}{2}, \frac{v}{2}\right)} \int_{-t}^{t} \left[1 + \frac{x^2}{v}\right]^{-\frac{v+1}{2}} dx \tag{8}$$

Experimental design: The response surface methodology provides explicit functions to represent the relationship between several explanatory or design variables and one or more response variables, using a set of experiments designed with a DOE technique. The main advantage of using this approach is the significant reduction in the number of numerical/physical experiments required to explore the design space. Once the response surfaces of the problem have been obtained, the algorithm is applied to these functions. In other words, instead of directly optimizing on the equation derived from the problem's finite element discretization, optimization is performed

on the functions that relate the input variables to the output variables.

Therefore, the purpose of the experimental design is to obtain a representative data set. For this purpose, the OSF sampling method was used. The response surface was formulated using Kriging, a metamodeling algorithm suitable for highly non-linear responses. This method uses refinement points to support the solution, and these are determined when the error decreases by 3%. First, the refinement finds new design points and then the output parameter values are evaluated with the previous response surface. Subsequently, the actual values of the output parameters are calculated (numerical substitution) and finally, the response surface is updated with the new values.

There are several means of searching for the minimum value, including gradient-based methods, direct search methods, and genetic algorithms. Hybrid methods also exist. The problem to be solved in this study is multi-objective. That is, several objective functions are to be minimized. The first authors to recognize multi-objective problems were Edgeworth and De Weck [24] and, at the beginning of the twentieth century, Pareto [25]. To deal with multi-objective problems, traditional gradient-based optimizers use aggregation function approaches, which use addition, multiplication or any other combination of arithmetic operations to combine all of the objectives into one. The problem lies with defining how the combination is performed. Due to the difficulty of conventional optimization techniques when extended to multi-objective optimization, a multi-objective genetic algorithm (MOGA) was chosen.

Evolutionary algorithms, such as the Genetic Algorithm (GA), are appropriate for this type of problem since they search for a set of parallel solutions such that, using some modifications of the operators used by GAs, the search process can be driven towards a family of solutions that represent the set of Pareto optimal solutions. The second version of the Niched Strength Genetic Algorithm (NSGA II) was used [26].

MOGAs provide a more refined approach, thus avoiding falling into a local minimum. They identify global and local minimums, provide multiple candidates in different regions, and can simultaneously handle multiple targets [27, 28]. The number of initial samples should be 10 times the number of continuous input parameters. While the larger, the better, it is more time consuming and the number of samples per iteration should be equal to or greater than the number of input and output parameters, but equal to or less than the number of initial samples. Hence, the importance of the parameter correlation study.

2.4 Description of the numerical models

Beginning with the geometry of the previous analysis, the number of defined parameters remains the same. The problem was solved, and a 2D stress analysis was performed considering the geometry of the WAHP, and the panel formed by surfaces. The quality of the mesh was acceptable (0.992 average quality where 1 is perfect) for the CZM analysis and, after possible debonding, an *augmented Lagrange contact approach* was used. For this, the mesh was mapped between the contacted surfaces and forced to a size of 1 mm. The most sensitive areas are the extreme regions of the contact.

The output parameter to be minimized was the Von Mises stress of the WAHP. In addition, distinct trajectories and points were added to control the stress and displacement at certain points that are the most sensitive to failure (Fig. 6). The stress studied in the WAHP was limited to the yield stress of the material since the plastic behaviour of the structures is not considered in the naval calculation. For this, a displacement of 25 mm was imposed at the free end of the hybrid panel.

3 Testing method

The validation of the numerical result requires an experimental study; ten (10) specimens were prepared with the geometry resulting from the simulation, to compare the results obtained. Once the model is validated, the numerical results of the joint can be considered reliable.

A model ME-40615 Servosis machine was used. The test setup is shown in Fig. 7. The clamping on the left side of the specimen was ensured with bolted steel jaws, simulating an embedment. A vertical load was applied to the opposite side with a roller so that the load was uniformly applied across the specimen's width, and it was tested over the displacement magnitude applied in the numerical simulation. The
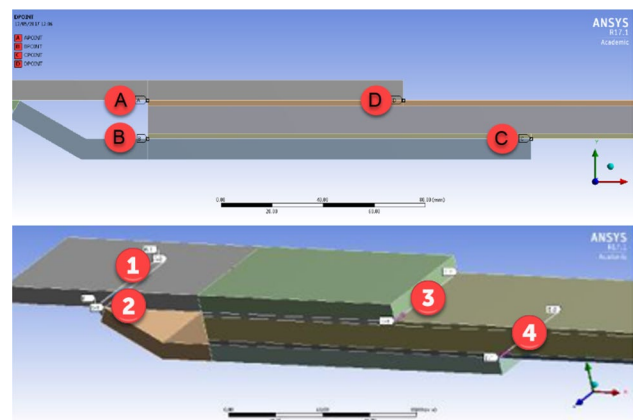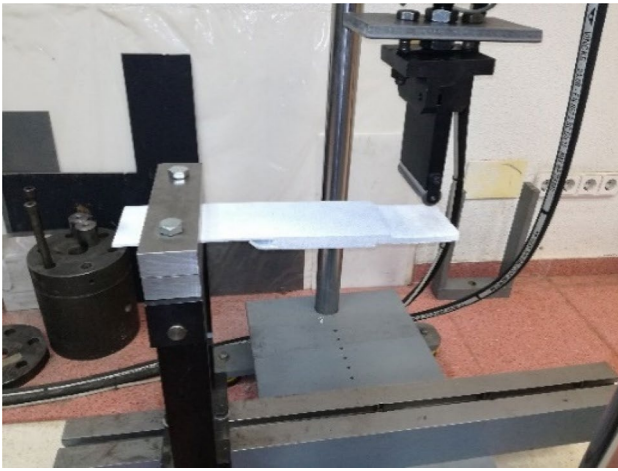

Fig. 6 Control points and paths for debonding analysis

Fig. 7 Test set up

tests were carried out with an increasing load until reaching a maximum displacement of 50 mm, with a load application speed of 3 mm/min. After the test, a visual inspection was carried out on each specimen.

The image correlation process used to obtain the displacement data requires that the specimen be prepared properly. A white paint base is applied to the study areas, and once drying, the control points are placed on it. The control points allow us to follow the specimen's behaviour in a step-by-step manner. The video of the experiment was processed by recording the displacements of each of the points and then translating it numerically.

3.1 Materials

The two-component adhesive was prepared and cured at room temperature. The quantities of each component were 100 ml of *component 1* per 25 ml of *component 2*. A curing time of 2.5 h was used for each bond to ensure perfect adhesive curing. The adhesive used in the fabrication was

Sika 7710 L100 [29], the properties of which are listed in Tables 3 and 4.

Mateglass Pro-3 was used for the panel. It is a hybrid material in resin laminates requiring high stiffness. The material has a core that allows high speed resin flow and is typically used in structures requiring simplicity and fast curing, with no compromise in quality or mechanical properties. Table 5 shows the properties extracted from the data sheet of the materials used.

A Mateglass layer is composed of the materials described below: Mat, Woven Roving, and Procore. The layer is symmetrical, and, therefore, one layer of material consists of a Mat, Woven roving, 90º orientation, nylon, multiaxial ± 45º, and another Mat. Three layers of 3 mm thickness were used to manufacture the sample.

Naval steel was used. The plastic approach of the isotropic hardening (bilinear hardening stress) used is shown in Fig. 8.

3.2 Specimens

The WAHP specimen consisted of two 4 mm thick steel sheets. The specimen width was limited to 100 mm. The upper lip of the specimen was longer than the lower lip, due to the numerical analysis, and it was clamped to a fixed point (Fig. 9) in the left area by means of a jaw. Ten specimens were constructed.

Different steps were followed to fabricate each specimen; the surfaces of the two steel skins were pre-treated with shot-blasting (corundum) before the adhesive was applied, and the adhesive was spread in three layers before the Mateglass was cured.

Once the first layer of Mateglass was adhered to the steel, the vacuum process for the application of the resin was initiated. After 24 h, the sample was deemed ready. A total of 3 kg per square meter of resin was used. The resin was mixed with the cobalt octoate activator (750 g of resin and 2.25 g of activator). Once the exothermic reaction

**Table 3** Adhesive physical properties

	Component A: SikaForce-7710 L100	Component B: SikaForce-7010
Physical properties		
Chemical base	Polyols, filled	Isocyanate derivatives
Colour (CQP 001-1)	Beige	Brown, transparent
Colour mixed	Beige	
Curing mechanism	Poly addition	
Density (CQP 006-4)	1.6 g/cm^3	1.2 g/cm^3
Density mixed (calculated)	1.5 g/cm^3	
Mixing ratio by volume	100	25
By weight	100	19
Solids content	100%	100%

Table 4 Adhesive mechanical properties

	Component A: SikaForce-7710 L100	Component B: SikaForce-7010
Mechanical properties		
Viscosity (CQP 538-2)	30,000 mPa·s	250 mPa·s
Viscosity mixed (CQP 538-2)	10,000 mPa·s	
Pot life (CQP 536-3)	100 min	
Application temperature range	15–30 °C	
Application time	50 min	
Open time (CQP 590-1)	100 min	
Press time (CQP 590-1)	230 min	
Shore D hardness	80 D	
Tensile strength	13 N/mm^2	
Elongation at break	8%	
Tensile shear strength	9 N/mm^2	
Numerical properties for simulation		
Debonding interface mode	Mixed	
Max. normal contact stress	28 MPa	
Critical fracture energy for normal separation	390 Jm^2	
Max. equivalent tangential contact stress	28 MPa	
Critical fracture energy for tangential slip	700 Jm^2	

Table 5 Mateglass Pro-3 properties

| Composition	M500WRS900PC (1) BX1000M500/125	
Technical data		
Composition	E-glass	
Weight per unit	g/m^2	3000
Tolerance	%	±7
Thickness (dry)	mm	4
Composition:		
Layer 1: Mat	Weight (g/m^2)	500
	Length	50 mm/38 tex
Layer 2: woven roving	Weight (g/m^2)	900
Layer 3 PROCORE	Weight (g/m^2)	100
Thickness	mm	1
Layer 4: multiaxial		
type: ±45°	Weight (g/m^2)	1000
Layer 5: Mat	Weight (g/m^2)	500
	Length	50 mm/38tex
Seam: PES 110D	g/m^2	
Type of seam	trico, galga 3.5	16
Width (std)(1)	cm	125
Tolerance	%	±1.5
UP and EP Resin		
Agent	silane	<0.15
Humidity	%	–
Full length	m	76
Numerical properties		
Young's modulus	Mpa	3780
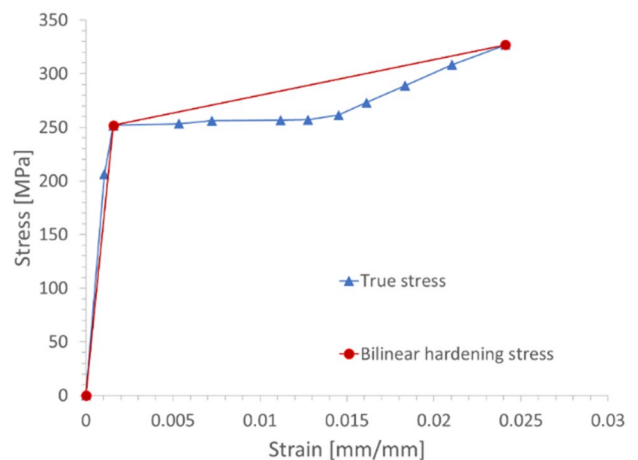
Fig. 8 Isotropic hardening of the steel

began, the resin cured after 50 min. The last step was to weld the lower lip at the exact location of the optimization study.

The welding between the lips of the part was carried out via MIG-MAG, using 6 V and a wire speed of 3.5 mm/min. Only a very small area was affected by the heat and it did not affect either the adhesive or the Mateglass. The gases used were 85% Argon and 15% CO_2 and the steel wire was S360 anti-spatter. The final step of the specimen preparation was the painting of the control points (Fig. 10).

Fig. 9 Specimen dimensions (mm)
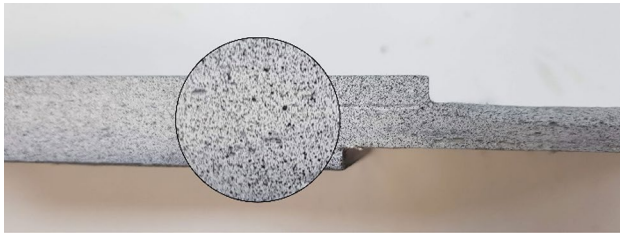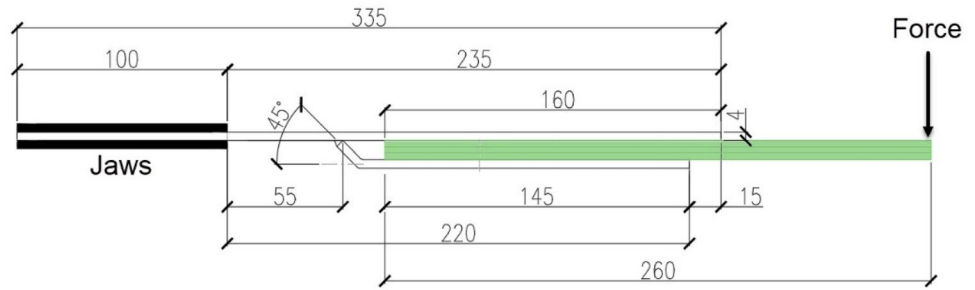
Fig. 10 Manufactured study specimen and black painted spots

3.3 Image correlation (NCorr)

Photographs were taken during the test and were videotaped for the post-processing of the images by correlation. The NCorr code [30] was used to verify the displacement of the control points for each specimen frame by frame. The algorithm tracked each point and Matlab was used to translate them in terms of displacement and deformation. Initially, a calibration was performed with each specimen at rest, and then the videos were processed.

4 Results

4.1 Topological optimization results

Figure 11 shows the results obtained in the 2D topological optimization for the mass ranges of 0.7 and 0.3, respectively. The material not shown in Figs. 11 and 12 could be removed without altering the Von Mises stress and displacement solutions. A similar result was obtained with the 3D simulation.

For the mesh quality in the 3D simulation, an average of 0.88 was obtained for the entire model, reaching a value of 1 for most of the elements (blue bar on the right in Fig. 13).

4.2 Non-linear simulation results

The objectives to be minimized were the Von Mises stress and three candidates that input parameters are different were found for the solution. The candidate that minimized the stress both globally and at the control points was selected.
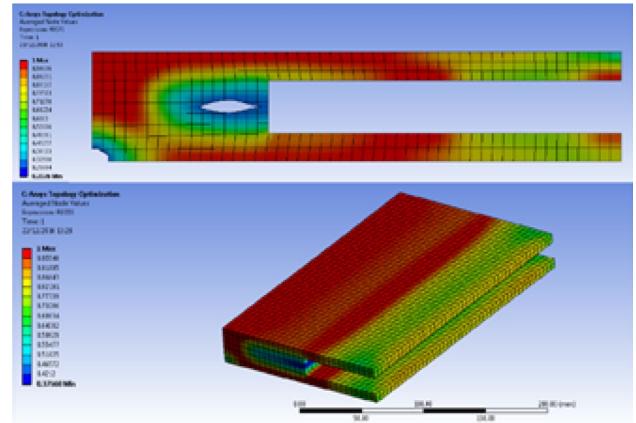
Fig. 11 2D vs. 3D topologic results for the mass reduction range of 0.3
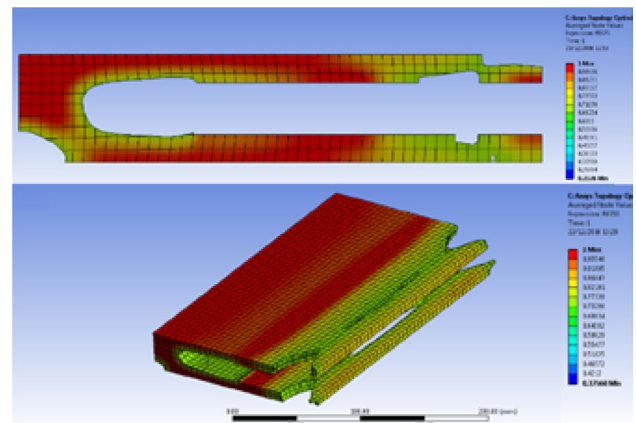
Fig. 12 2D vs. 3D topologic results for the mass reduction range 0.7

Its dimensions are shown in the following table, with the numerical solutions being rounded to manufacturable solutions (Table 6).

The maximum Von Mises stresses found in the simulation were 149.00 MPa for candidate I, 141.19 MPa for candidate II, and 145.11 MPa for candidate III. In control points C and D and in the path studied between them, no. 3 and no. 4
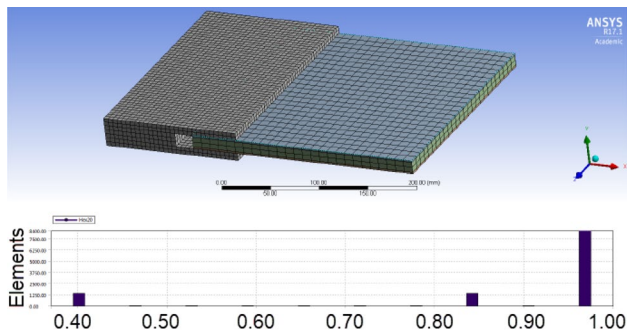
Fig. 13 3D Mesh quality

Table 6 Theoretical and constructive parameter solution

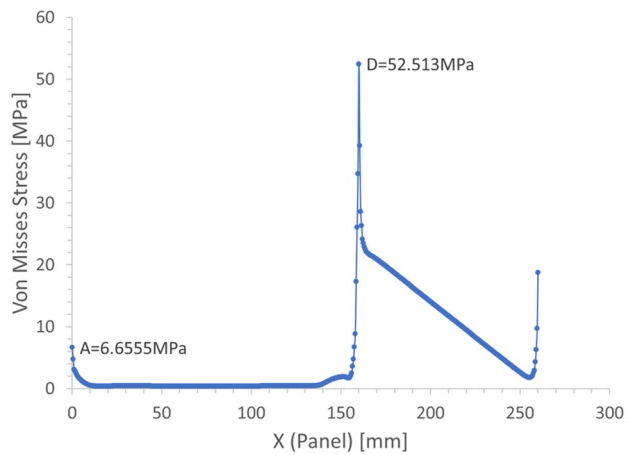| Parameter	Units	Theoretical	Constructive
UL	mm	234.85	235
OL	mm	154.664	160
LL	mm	223.58	220
A	°	44.850	45
WL	mm	54.505	55
WF	mm	7.770	7.7

Fig. 14 Von Mises result in adhesive area below upper lip (WAHP)

according to Fig. 6, the following stresses were observed in candidate II (Upper adhesive overlap D-point 52.51 MPa), working in the elastic regime (Fig. 14).

4.3 Laboratory test results

The deformations found during Matlab processing agree quite well with those found in the non-linear numerical model, in Fig. 15 the upper image dark blue represents the maximum displacement of 25 mm; in the lower image dark
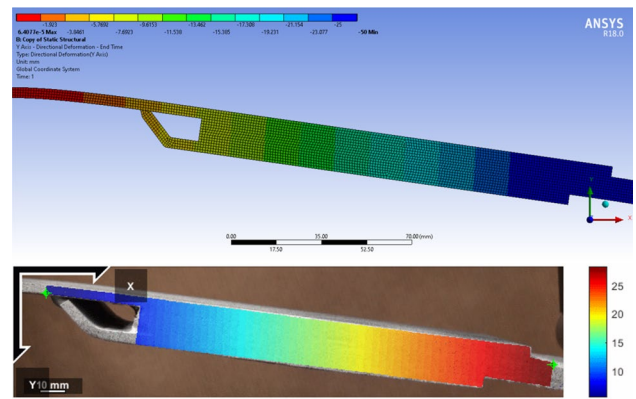
Fig. 15 Deformation in mm processed by numerical simulation vs. NCorr
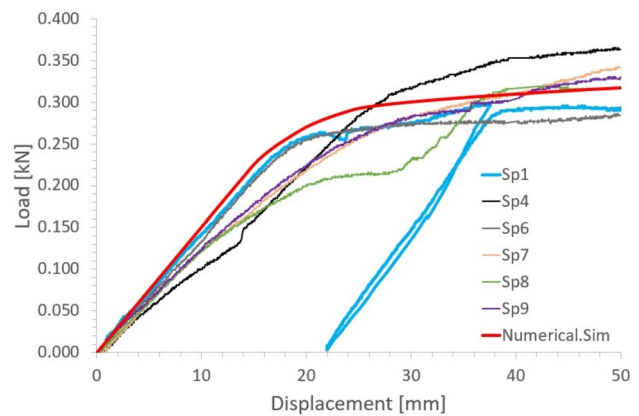
Fig. 16 Load applied vs. deformation processed

red represents the maximum displacement 25 mm. One of the NCorr processed data is shown in Fig. 16.

5 Discussion of results

The topological optimization results are similar in the 2D and 3D models. There is an area in the center of the block between the upper and lower lips of low stress level that is subject to suppression in the result of this phase. The same occurs in the lower area under the embedment. Therefore, the geometry adopted after the topological optimization phase can be interpreted as follows, based on the initial assumptions: two steel sheets welded in a C-shape under an angle at the lower lip; the solution is easy to produce, since steel sheets are readily available in shipyards around the world and are cheaper than starting casting. Manufacturing a casting is more expensive than using two plate elements with a weld between them. Furthermore, the shipyard does not have to train personnel for assembly, since plates are

welded together in a conventional manner, and the prefabricated panel can even be delivered with the joint prior to assembly on the yard.

From the 2D/3D analysis, it is observed that the solution is independent of the width of the part (a), see Figs.11 and 12; the upper plot (2D) corresponds to a 50 mm value and the lower one (3D) to a 250 mm; and a small area exists at the end of the upper lip that is not subjected to load. This led to different consideration of the lip lengths in the non-linear simulation. It is possible to make a chamfer in the area as a construction detail.

As for the non-linear simulation, one of the difficulties of the problem lies in the good modelling of the fracture zone with the subsequent contact, since the model must converge for any value of the parameters. To reduce the processing time, the initial number of experiments in the optimization was reduced to 50 using parameter correlation. However, the results obtained were sufficiently accurate, since the sample was subsequently refined and verified. As for the sensitivity of the candidate solution parameters, it can be concluded that the WAHP is most sensitive to all welding-related parameters. The most affected are the plate welding angle and weld foot dimension. The upper lip length parameter is not a determining parameter.

The parameter sizes between all the candidates were very similar, offering Von Mises results with a difference of 5.2% between candidate I and the chosen one, and of 2.8% with candidate III. Since it was observed that the initial debonding zone occurred at control point D, the proposed solution also minimizes this stress. Therefore, the WAHP will have more margin for a possible debonding since this is the point revealing fracture propagation in the simulations [20]. The uncertainties in input parameters of the numerical model may explain some of the differences found in the deformations processed versus the numerical approach (Fig. 16).

The numerical approach was carried out using a 2D non-linear model. The comparison between the simulation and the experimental results of the clamp specimens suitably validates the numerical model (Fig. 17), whose results remain within the margins of variability found in the laboratory tests. In Fig. 17, the green arrow shows the area where plastic behaviour is observed in each specimen when exceeding the elastic limit.

The specimen is found to suffer less stress around the adhesive bond. Everything is transmitted to the steel around the embedment and all of the pieces behave in the same way. The numerical simulation presents the same results, 52.40 MPa Von Mises, in the area where the steel ends at the upper lip, and the Mateglass. The maximum over time is found in the embedded area, with a value of 355.48 MPa. This value is over yield stress.

In the finite element model of the bond with the cohesive law, the maximum stress found at the upper lip end is
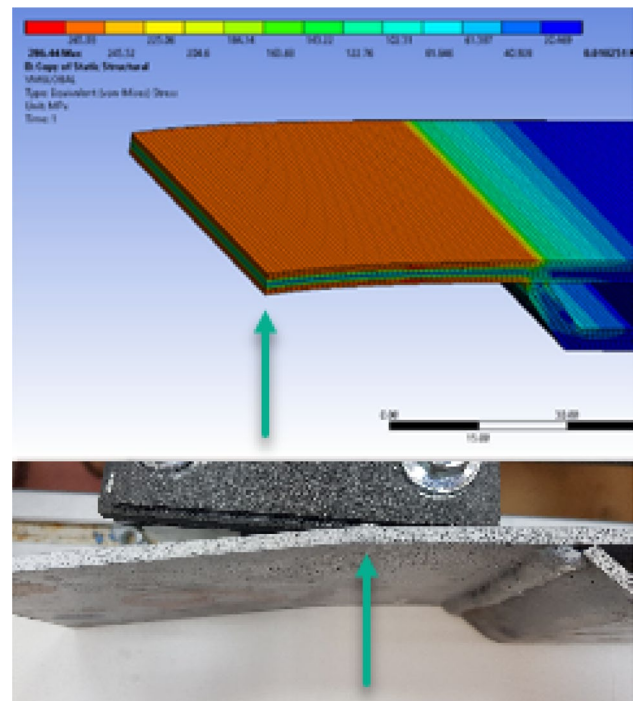

Fig. 17 Numerical model vs. laboratory test. Notice that the green arrow points the limit of the clamped boundary conditions
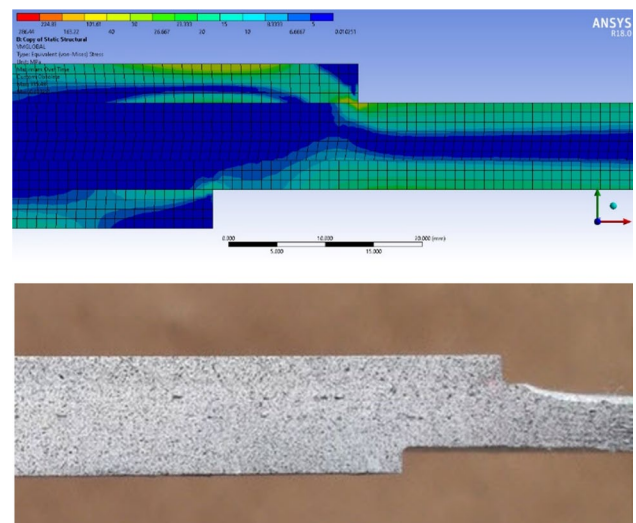
Fig. 18 No inter-laminar crack propagation in the upper lip nor in the lower lip. (52.4 MPa max. stress)

52.40 MPa, and this value does not exceed the adhesive's debonding stress. This phenomenon is also observed during the laboratory experiment, since no specimen presented debonding or cracking, Fig. 18.

The behaviour of the specimens, as compared to the numerical model (red line in Fig. 16), is very similar in the linear zone, where the deviation between the deformation
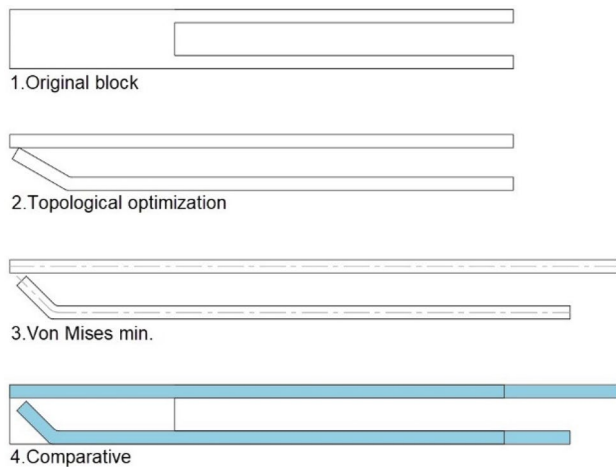
Fig. 19 Comparative between initial cast part and solution

and the applied force is quite small. The shape of the graphs remains parallel until the plastic behaviour begins. Here, the differences between the specimens and the simulation differ to a greater or lesser extent, depending on manufacturing and/or test imperfections. Furthermore, it is observed that the slope of the graph matches with the steel used. Therefore, it is deduced that all of the stress is supported by the steel plate at its junction with the jaws, Fig. 17. In Fig. 16, in the behaviour curve of the first specimen (marked in blue), it can be seen that, when unloaded, the behaviour is parallel to the initial slope and when it is reloaded, it returns with accumulated plastic damage.

The deviations between the constructive parameters and the theoretical parameters of the simulation are negligible in the result. The comparison between the result and the initial seed is presented in Fig. 19.

6 Conclusion

The designed joint geometry is easy to produce, install and carry out in any shipyard. Therefore, the competitiveness of a structural system using panels is increased. The weight after parametric optimization and Von Mises stress minimization is 16.4% less than that of the initial solution. Furthermore, by linking the numerical behaviour of the simulation with the behaviour of the experiment, the results of the numerical optimization are considered acceptable and valid for the definition of the WAHP in the elastic regime, since shipbuilding always considers linear material behaviour, and since no cracks or imperfections were observed in the panel's adhesive bond.

References

1. Terndrup Pedersen P (2015) Marine structures: future trends and the role of universities. Engineering 1(1):131. https://doi.org/10.15302/J-ENG-2015004
2. Seo Y, Sheen D, Kim T (2007) Block assembly planning in shipbuilding using case-based reasoning. Expert Syst Appl 32(1):245–253. https://doi.org/10.1016/j.eswa.2005.11.013
3. I. G. of Authorities, Ship Design and Construction (2003)
4. SAND.CORe Coordination Action on Advanced Sandwich Structures in the Transport Industries Under European Commission Contract No. FP6-506330 (2013) Best Practice Guide for Sandwich Structures in Marine Applications, pp 279
5. de Vicente M, Rodrigo PF, Fernández MT (2019) Structural design of helicopter deck with hybrid materials and its joints with conventional steel. Mar Struct 2019:359–368
6. Kozak J (2010) Selected problems on application of steel sandwich panels to marine structures. Polish Marit Res 16(4):9–15. https://doi.org/10.2478/v10012-008-0050-4
7. Det Norske Veritas (2019) DNVGL-ST-C501 Composite Components, no. November, p 250 [Online] Available: http://exchange.dnv.com/publishing/codes/docs/2013-11/OS-C501.pdf
8. Noury P, Hayman B, McGeorge D, Weitzenböck JR (2002) Lightweight construction for advanced shipbuilding—recent development. In: 37th WEGEMT summer sch, pp 1–23
9. Watson DGM (1998) Practical Ship Design (Elsevier Ocean Engineering), vol 1
10. Partner R (2020) Engineering, production and life-cycle management for the complete construction of large-length FIBRE-based SHIPs D2. 6 (WP2): Guidance for the use of composite materials in large length ships, vol 6, pp 1–79
11. Wp D, Rules C (2020) Engineering, production and life-cycle management for the complete construction of large-length FIBRE-based SHIPs | FIBRESHIP Project | H2020 | CORDIS | European Commission, vol 3, [Online]. https://cordis.europa.eu/project/id/723360/es
12. DNV GL (2016) DNVGL-CG-0154 CLASS GUIDELINE Steel sandwich panel construction
13. Lloyds Register of Shipping (2006) Provisional rules for the application of sandwich panel construction to ship structure. April 2006

14. Kozak J, Niklas K (2015) FEM modelling of stress and strain distribution in weld joints of steel sandwich panels. Weld Int 29(10):783–787. https://doi.org/10.1080/09507116.2014.937597

15. Anyfantis KN (2012) Finite element predictions of composite-to-metal bonded joints with ductile adhesive materials. Compos Struct 94(8):2632–2639. https://doi.org/10.1016/j.compstruct.2012.03.002

16. Jen YM, Chang LY (2008) Evaluating bending fatigue strength of aluminum honeycomb sandwich beams using local parameters. Int J Fatigue 30(6):1103–1114. https://doi.org/10.1016/j.ijfatigue.2007.08.006

17. Boukharouba W, Bezazi A, Scarpa F (2014) Identification and prediction of cyclic fatigue behaviour in sandwich panels. Meas J Int Meas Confed 53:161–170. https://doi.org/10.1016/j.measurement.2014.03.041

18. Harilal R, Ramji M (2014) Adaptation of open source 2D DIC software Ncorr for solid mechanics applications. In: 9th international symposium on advanced science and technology in experimental mechanics, 2014, November, pp 1–6, https://doi.org/10.13140/2.1.4994.1442

19. ANSYS Inc. (2013) ANSYS Meshing User's Guide

20. De Vicente M (2018) Numerical optimization of hybrid panel joints by mixed adhesive/welded method on shipbuilding. In: OMAE-2018, pp 1–11

21. Banea MD, da Silva LFM (2009) Adhesively bonded joints in composite materials: an overview. Proc Inst Mech Eng Part L J Mater Des Appl 223(1):1–18. https://doi.org/10.1243/14644207JMDA219

22. Budhe S, Banea MD, de Barros S, da Silva LFM (2017) An updated review of adhesively bonded joints in composite materials. Int J Adhes Adhes 72:30–42. https://doi.org/10.1016/j.ijadhadh.2016.10.010

23. Alfano G, Crisfield MA (2001) Finite element interface models for the delamination analysis of laminated composites: mechanical and computational issues. Int J Numer Methods Eng 50(7):1701–1736. https://doi.org/10.1002/nme.93

24. De Weck O (2004) Multiobjective optimization: history and promise. In: Proc. 3rd China-Japan-Korea Jt. Symp. Optim. Struct. Mech. Syst. Invit. Keynote Pap. GL2–2, p 14. https://doi.org/10.1109/TEVC.2009.2017515

25. Pareto V, Montesano A (2014) Manual of political economy: a critical and, variorum edn. Oxford University Press, Oxford

26. Deb K, Pratap A, Agarwal S, Meyarivan T (2002) A fast and elitist multiobjective genetic algorithm: NSGA-II. IEEE Trans Evol Comput 6(2):182–197. https://doi.org/10.1109/4235.996017

27. Deb K (2011) Multi-objective optimization using evolutionary algorithms: an introduction. Accessed 19 Dec 2016. [Online]. http://www.iitk.ac.in/kangal/deb.htm

28. Deb K (2010) Multi-Objective Optimization using Evolutionary Algorithms, vol 13. John Wiley and Sons, Hoboken

29. Sheet PD, Data TP, Benefits P (2011) SikaForce-7710 L100 (formerly 1899) General purpose sandwich panel adhesive, vol 100 (formerly 1899)

30. Blaber J, Adair B, Antoniou A (2015) Ncorr: open-source 2D digital image correlation Matlab Software. Exp Mech 55(6):1105–1122. https://doi.org/10.1007/s11340-015-0009-1